











## Article

# Prediction of Protein Targets in Ovarian Cancer Using a Ru-Complex and Carbon Dot Drug Delivery Therapeutic Nanosystems: A Bioinformatics and $\mu$ -FTIR Spectroscopy Approach

Maja D. Nešić<sup>1,\*</sup>, Tanja Dučić<sup>2,\*</sup>, Branislava Gemović<sup>3</sup>, Milan Senčanski<sup>3</sup>, Manuel Algarra<sup>4</sup>, Mara Gonçalves<sup>5</sup>, Milutin Stepić<sup>1</sup>, Iva A. Popović<sup>1</sup>, Đorđe Kapuran<sup>1</sup> and Marijana Petković<sup>1</sup>

<sup>1</sup> Center for Light-Based Research and Technologies COHERENCE, Department of Atomic Physics, Vinča Institute of Nuclear Sciences, National Institute of the Republic of Serbia, University of Belgrade, 11000 Belgrade, Serbia; mstepic@vin.bg.ac.rs (M.S.); ivavukicevic@vin.bg.ac.rs (I.A.P.); djordje.kapuran@vin.bg.ac.rs (Đ.K.); marijanapetkovic@vin.bg.ac.rs (M.P.)

<sup>2</sup> ALBA-CELLS Synchrotron, 08290 Cerdanyola del Vallès, Spain

<sup>3</sup> Laboratory for Bioinformatics and Computational Chemistry, Vinča Institute of Nuclear Sciences, National Institute of the Republic of Serbia, University of Belgrade, 11000 Belgrade, Serbia; gemovic@vin.bg.ac.rs (B.G.); sencanski@vin.bg.ac.rs (M.S.)

<sup>4</sup> INAMAT2—Institute for Advanced Materials and Mathematics, Department of Science, Public University of Navarre, Campus de Arrosadia, 31006 Pamplona, Spain; manuel.algarra@unavarra.es

<sup>5</sup> CQM—Centro de Química da Madeira, Universidade da Madeira, 9020-105 Funchal, Portugal; maraisabel@staff.uma.pt

\* Correspondence: maki@vin.bg.ac.rs (M.D.N.); tducic@cells.es (T.D.); Tel.: +38-1113408770 (M.D.N.)



**Citation:** Nešić, M.D.; Dučić, T.; Gemović, B.; Senčanski, M.; Algarra, M.; Gonçalves, M.; Stepić, M.; Popović, I.A.; Kapuran, Đ.; Petković, M. Prediction of Protein Targets in Ovarian Cancer Using a Ru-Complex and Carbon Dot Drug Delivery Therapeutic Nanosystems: A Bioinformatics and  $\mu$ -FTIR Spectroscopy Approach. *Pharmaceutics* **2024**, *16*, 997. <https://doi.org/10.3390/pharmaceutics16080997>

Academic Editors: Xiaoyong Wang, Ionela Andreea Neacsu and Ecaterina Andronescu

Received: 10 June 2024

Revised: 18 July 2024

Accepted: 25 July 2024

Published: 27 July 2024



**Copyright:** © 2024 by the authors. Licensee MDPI, Basel, Switzerland. This article is an open access article distributed under the terms and conditions of the Creative Commons Attribution (CC BY) license (<https://creativecommons.org/licenses/by/4.0/>).

**Abstract:** We predicted the protein therapeutic targets specific to a Ru-based potential drug and its combination with pristine and N-doped carbon dot drug delivery systems, denoted as RuCN/CDs and RuCN/N-CDs. Synchrotron-based FTIR microspectroscopy ( $\mu$ FTIR) in addition to bioinformatics data on drug structures and protein sequences were applied to assess changes in the protein secondary structure of A2780 cancer cells.  $\mu$ FTIR revealed the moieties of the target proteins' secondary structure changes only after the treatment with RuCN and RuCN/N-CDs. A higher content of  $\alpha$ -helices and a lower content of  $\beta$ -sheets appeared in A2780 cells after RuCN treatment. Treatment with RuCN/N-CDs caused a substantial increase in parallel  $\beta$ -sheet numbers, random coil content, and tyrosine residue numbers. The results obtained suggest that the mitochondrion-related proteins NDUFA1 and NDUFB5 are affected by RuCN either via overexpression or stabilisation of helical structures. RuCN/N-CDs either induce overexpression of the  $\beta$ -sheet-rich protein NDUF51 and affect its random coil structure or interact and stabilise its structure via hydrogen bonding between -NH<sub>2</sub> groups from N-CDs with protein C=O groups and -OH groups of serine, threonine, and tyrosine residues. The N-CD nanocarrier tunes this drug's action by directing it toward a specific protein target, changing this drug's coordination ability and inducing changes in the protein's secondary structures and function.

**Keywords:** nano-based anticancer drug delivery systems; protein targets; carbon dots; bioinformatics;  $\mu$ FTIR

## 1. Introduction

Epithelial ovarian cancer accounts for 90% of all ovarian cancer diagnoses and is one of the most frequent and lethal types of gynaecological malignancies worldwide [1]. There are multiple reasons, including asymptomatic behaviour, diagnosis at advanced stages of the disease, recurrence, and resistance to chemotherapy, for this high mortality rate. Consequently, exploring new potential therapeutic targets related to overcoming drug resistance mechanisms and new treatment strategies is of great need for ovarian cancer patients. Nanotechnology is a part of the solution since the number of nano-based

treatments and components for cancer-oriented theranostic techniques in clinical use has progressively increased [2]. Cancer nanomedicine predominantly focuses on improving pharmacokinetics and pharmacodynamics, targeting capability, and increasing localised drug efficacy [3]. Furthermore, enhanced therapeutic specificity can help eliminate the systemic toxicities associated with traditional therapies and improve prognosis and patient quality of life. Nanoformulations that fulfil all the tasks mentioned above, are nanocarriers (NCs) for anticancer drugs, which can act based on passive and/or active targeting [4]. For example, NCs can be designed to release drugs under external stimulation, such as illumination, magnetic field, and hyperthermia, a process known as active targeting. On the other hand, passive targeting and local drug activation are based upon specific cancer-sounding conditions such as pH, oxidative/reductive environments, and enhanced permeation and retention (EPR), wherein NCs can predominantly accumulate within tumour tissue [5]. Moreover, NCs can be designed to tune the mechanism of a drug's action by interacting with specific biomolecule targets.

In the past few years, molecular targets and signalling pathways specific to cancer cells have been identified, enabling the development of new treatment strategies with advanced efficacy, selectivity, and reduced systemic toxicity. Along with nucleic acids, proteins have been recognised as drug targets for cancer therapeutics since they are essential in cancer cell growth, differentiation, metabolism, and survival. Proteins specific for cancer cells and those overexpressed in cancer cells stand out as potential drug targets. Some are membrane receptors, while others are markers on the cancer cell surface or overactive enzymes involved in specific signalling networks that promote or sustain cancer development [6–10]. Overexpressed membrane receptors or markers can serve as targets for drug docking and/or specific cell penetration of a drug.

On the other hand, overexpression of some specific enzymes, e.g., cyclin-dependent kinases (CDK4, CDK6, and CDK2), polo-like kinase 1 (PLK1), and aurora kinases (aurora A and aurora B), can induce or contribute to tumorigenesis, which drives cancer progression [10,11]. Targeting these signalling pathways and proteins responsible for cancer progression has become the primary strategy used in developing new drug therapies approved by multiple regulatory authorities (e.g., the European Medicines Agency (EMA), the U.S. Food and Drug Administration, the FDA). Therefore, choosing a suitable drug carrier could help tune drug properties to target key proteins. Although much experimental research has been conducted in the past decades, identifying drug–protein interactions remains tedious and time-consuming. Computational approaches have been developed to predict biological targets that can improve drug discovery success rates and simultaneously reduce experimental time and costs.

This study aims to explore the changes in the proteins of ovarian cancer cells caused by a potential drug Ru-complex (RuCN) and nanosystems made of NCs, carbon dots (CDs), and N-doped carbon dots (N-CDs) and RuCN, denoted as RuCN/CDs and RuCN/N-CDs. A Ru complex with an  $\eta^5$ -cyclopentadienyl ligand,  $[\text{Ru}(\eta^5\text{-C}_5\text{H}_5)(\text{PPh}_3)_2\text{CN}]$ , was selected according to its attractive photochemical and pharmacological properties for cancer therapy [12–14]. Recently, it was shown that ruthenium cyclopentadienyl complexes could act as protein kinase inhibitors and reactive compounds, which can induce the cleavage of protection groups in a biological environment [15–17]. CDs and N-CDs were used as NCs since they possess all the required properties: surfaces that can be easily modified and functionalised to interact with drug functional groups and biomolecules, high water dispersity, and good biocompatibility. This system showed promising potential for photodynamic therapy against CAL72 and A2780 cancer cell lines [18]. However, its mechanism of action without light activation has not been investigated in detail. Therefore, in this study, we used synergy between computational biology and FTIR spectroscopy to address the influence of RuCN with and without NCs on protein structure and function in the A2780 cancer cell line, which was used as a model system for human epithelial ovarian cancer.

In this study, we employed a computational evaluation of protein structures and an experimental approach involving the use of  $\mu$ FTIR to evaluate the effect of the analysed nanoparticles on total cellular protein status. We investigated the signalling pathways and protein–protein interaction (PPI) networks that are affected by the potential drug, RuCN, and nanotherapeutics based on RuCN and CDs or N-CD NCs (RuCN/CDs and RuCN/N-CDs), which are relevant to ovarian cancer. We aimed to assess the protein conformations and monitor any eventual conformational changes of secondary protein structures induced by the abovementioned treatments. To achieve this, we applied synchrotron-based Fourier transform infrared microspectroscopy ( $\mu$ FTIR), an effective and sensitive method for detecting proteins' secondary structures and managing the overall protein conformational changes occurring in cells when exposed to treatments. Furthermore, based on recorded structural changes of proteins in A2780 cells resulting from nanosystems, we discussed the role of (N-)CD NCs' surface chemistry and their effects on the complexity of the RuCN-mediated anticancer mechanism in the A2780 cancer cell type.

## 2. Materials and Methods

### 2.1. Materials

Organoruthenium complex, cyano( $\eta^5$ -cyclopentadienyl)bis(triphenylphosphine) ruthenium(II) [Ru( $\eta^5$ -Cp)(PPh<sub>3</sub>)<sub>2</sub>CN], denoted in the text as RuCN, was prepared and characterised according to established methods [13]. CDs and N-CDs were designed and characterised as previously described [19,20]. Nanocomposite systems made of RuCN and CDs or N-CDs (RuCN/(N-)CDs) were prepared by mixing RuCN with CDs or N-CDs over 24 h in a shaker at room temperature in the dark. Our previous publication described the structural arrangements of NPs and RuCN [18].

The A2780 human ovarian cancer cell line was obtained from the European Collection of Cell Cultures (ECACC, Salisbury, UK). The cell culture medium, foetal bovine serum (FBS), and antibiotics were purchased from Life Technologies (Paisley, UK).

### 2.2. Bioinformatics Analysis

The Informational Spectrum Method (ISM) was used to predict RuCN and (N-)CD protein targets in A2780 ovarian cancer cell line. ISM involves carrying out three major steps for prediction if two molecules are potential interactors: 1. Present molecules as a series of numbers based on Electron–Ion Interaction Potential (EIIP) [21]; in proteins, for example, each amino acid in the sequence of a protein's primary structure is replaced by the value of EIIP for that amino acid. 2. Then, transform this numerical sequence into an Informational Spectrum (IS) using Fourier Transform. 3. Finally, multiply the spectra of two molecules to generate a cross-spectrum (CS). If the peaks in the ISs of two molecules are at the same frequency, this could indicate their long-term molecular interaction, especially if the most pronounced peak in the CS of these two molecules is at the same frequency. Therefore, we used CSs of system components, RuCN, CDs, and N-CDs, paired with each of the A2780 proteins to predict the possible physical interactions. Step 1 of this procedure for RuCN, CDs, and N-CDs was conducted using the Informational Spectrum Method applied for Small Molecules (ISM-SM) described in [22].

### 2.3. Preparation of A2780 Cells for $\mu$ FTIR

A2780 cells were grown in RPMI-1640 medium containing 10% FBS and 1% antibiotic–antimycotic solution on a round 0.5 mm thick CaF<sub>2</sub> carrier and incubated with 12.5  $\mu$ M of RuCN containing 20  $\mu$ g/mL of either CDs or N-CDs for 24 h, as described in our previous publication [18]. Untreated cells were used as control. The samples were prepared and stored lyophilized in a dry atmosphere until  $\mu$ FTIR spectra acquisition. Lyophilisation results in a minimum contribution of water-related signals in FTIR spectra.

#### 2.4. Synchrotron Radiation Fourier Transform Infrared Micro-Spectroscopy ( $\mu$ FTIR)

The protein structures of A2780 cells before and after the treatment with RuCN, RuCN/CDs and RuCN/N-CDs were analysed using  $\mu$ FTIR (Synchrotron ALBA, MIRAS beamline, Barcelona, Spain). Synchrotron light was used as an IR source. A 3000 Hyperion microscope was coupled to a Vertex 70v spectrometer; mercury cadmium telluride (MCT) cooled with liquid nitrogen was used as a detector. The aperture of the FTIR microscope was set to the size of a single cell ( $12 \times 12 \mu\text{m}^2$ ), and fifty cells were analysed from each group. Three independent replicates were conducted by co-adding 256 spectra at  $4 \text{ cm}^{-1}$  resolution. The spectroscopic data were collected in transmission mode using the 36 Schwarzschild objective and condenser. Spectra for each treatment were collected in the  $4000\text{--}900 \text{ cm}^{-1}$  mid-IR range.

#### 2.5. Data Processing and Statistical Evaluation

The OPUS 8.2 (Bruker, Ettlingen, Germany) software was used for  $\mu$ FTIR data acquisition. Quasar software package Version 1.5.0. (Bioinformatics Laboratory of the University of Ljubljana, Slovenia) was employed to process protein region spectra, incorporating rubber band baseline correction and vector normalization for each spectrum. Second-derivative calculations were made by utilising a Savitzky–Golay filter with 15 smoothing points and a polynomial order of 3.

Statistical tests were performed with GraphPad Prism 7. Differences between means were considered significant when the  $p$ -value of the One-Way ANOVA test was less than 0.05.

### 3. Results and Discussion

#### 3.1. Predicting Targets and Underlying Therapeutic Mechanisms of RuCN, RuCN/CDs, and RuCN/N-CDs in A2780 Ovarian Cancer Cells

Specific signalling networks are known to promote or sustain cancer, and exploring hot spots in proteomic networks represents a suitable approach to developing target-specific therapeutics. In this work, we explore protein candidates that could serve as targets for RuCN, RuCN/CDs, and RuCN/N-CDs by using the Informational Spectrum Model (ISM). As a potential pool of protein interactors with RuCN, RuCN/CDs, and RuCN/N-CDs, we used protein products of genes with baseline expression in A2780 cells. For this, we downloaded the list of genes from Expression Atlas with  $\text{TPM} \geq 2.0$ , which was detected in the RNA-seq analysis of 934 human cancer cell lines (E-MTAB-2770) [23]. This list contained Ensemble identifiers of genes, but we needed the FASTA format of protein sequences for further research. We used the UniProt Retrieve/ID mapping tool to obtain 11 288 protein sequences that were further analysed as potential interactors with RuCN and CDs using the ISM [24].

ISM analysis showed that the tested N-CDs exhibited informational spectra identical to those of RuCN, with the dominant peak at a frequency of 0.016 (Figure 1a). Therefore, because the Ru-complex is a common part of both tested nanocomposite systems, we used RuCN as a model for cross-spectral analysis and paired it with each of the potential protein interactors in A2780 cells, assuming that the RuCN would target proteins in these cells [25,26]. The ISM analysis resulted in a list of 595 proteins with a dominant peak in the CS with RuCN at a frequency of 0.016. Afterwards, we used these proteins in an enrichment analysis conducted using the DAVID (Database for Annotation, Visualisation, and Integrated Discovery) tool to determine which pathways/Gene Ontology (GO) terms were enriched in this list [27]. Functional annotation clustering revealed that mitochondrion-related proteins were the cluster with the highest enrichment score, namely, 4.96 (Table 1). This cluster encompasses proteins associated with keywords such as “respiratory chain”, with 14 proteins from our list ( $p = 2.6 \times 10^{-6}$ , after Benjamini correction), and “mitochondrion inner membrane”, with 19 proteins from our list ( $p = 2.0 \times 10^{-2}$ , after Benjamini correction). This cluster’s most abundant protein groups were NADH dehydrogenases and mitochondrial ribosomal proteins (Table 1). The cluster with chromatin-related proteins

also had an enrichment score higher than 4.00 (Table S1) and encompasses proteins related to keywords such as “nucleosome core”, with 13 proteins from our list ( $p = 3.9 \times 10^{-4}$ , after Benjamini correction), and “chromosome”, with 26 proteins from our list ( $p = 8.6 \times 10^{-3}$ , after Benjamini correction). The most abundant proteins in this cluster are histones, as indicated in Table 1.

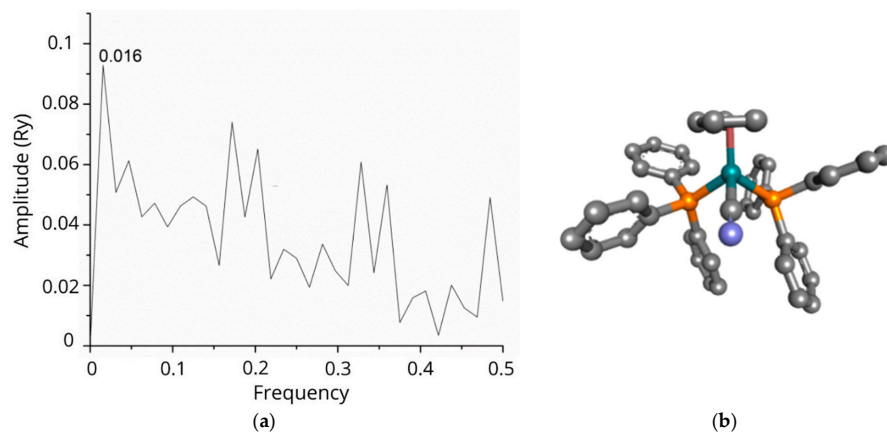


**Figure 1.** The informational spectrum of RuCN has a dominant peak at a frequency 0.016 (a). The molecular structure of the RuCN is given in (b), in which the cyan blue colour denotes the Ru-central metal ion, grey represent carbon-atoms, blue is the Cl, whereas the phosphorous atom is labelled with mustard colour.

**Table 1.** Cluster with highest DAVID enrichment score—mitochondrion-related proteins identified as potential targets of RuCN, with their secondary structures. Proteins coloured red are the ones with the highest percentages of  $\alpha$ -helices, and those in blue are the ones with the highest percentages of  $\beta$ -sheets.

Protein Group	Protein	Part of the Protein with a Known Secondary Structure	Secondary Structure	Contribution of $\alpha$ -Helices and $\beta$ -Sheets to the Protein Structure
NADH [ubiquinone] dehydrogenases	<b>NDUFA1</b>	1–70 (70 aa)	<b>5 helices</b> 11 helix–helix interactions, 5 beta turns, 1 gamma turn	<b>45.45%</b>
	NDUFA3	2–84 (84 aa)	<b>1 sheet</b> 1 strand <b>4 helices</b> 9 helix–helix interactions, 4 beta turns, 2 gamma turns	<b>8.30%</b> <b>33.33%</b>
	NDUFA8	4–172 (172 aa)	<b>1 sheet</b> 1 strand <b>7 helices</b> 14 helix–helix interactions, 17 beta turns, 4 gamma turns 1 disulphide	<b>3.22%</b> <b>22.58%</b>
	NDUFB1	3–58 (58 aa)	<b>4 helices</b> 10 helix–helix interactions, 6 beta turns	<b>40%</b>
	<b>NDUFB5</b>	52–189 (189 aa)	<b>6 helices</b> 20 helix–helix interactions, 5 beta turns, 2 gamma turns	<b>46.15%</b>
	NDUFB7	3–124 (137 aa)	<b>5 helices</b> 4 helix–helix interactions, 9 beta turns, 3 gamma turns, 1 disulphide	<b>29%</b>
	<b>NDUFS1</b>	30–716 (727 aa)	<b>6 sheets</b> 1 beta alpha beta unit, 6 beta hairpins, 3 beta bulges, 15 strands <b>27 helices</b> 33 helix–helix interactions, 82 beta turns, 14 gamma turns	<b>17.65%</b> <b>3.92%</b>
	NDUFS5	2–105 (106 aa)	<b>7 helices</b> 8 helix–helix interactions, 13 beta turns, 4 gamma turns, 2 disulphides	<b>26.92%</b>
	NDUFS6	29–123 (124 aa)	<b>2 sheets</b> 1 beta hairpin, 4 strands <b>2 helices</b> 1 helix–helix interaction, 11 beta turns, 1 gamma turn	<b>9.52%</b> <b>9.52%</b>

Table 1. Cont.

Protein Group	Protein	Part of the Protein with a Known Secondary Structure	Secondary Structure	Contribution of $\alpha$ -Helices and $\beta$ -Sheets to the Protein Structure
Mitochondrial ribosomal proteins	MRPL18	1–180 (180 aa)	<b>2 sheets</b> 2 beta hairpins, 1 beta bulge, 5 strands <b>5 helices</b> 12 helix–helix interactions, 12 beta turns, 3 gamma turns	6.66% 16.66%
	MRPL21	1–205 (205 aa)	<b>3 sheets</b> 3 beta hairpins, 5 beta bulges, 10 strands <b>1 helix</b> 1 helix–helix interaction, 11 beta turns, 1 gamma turn	8.82% 2.94%
	MRPL36	1–103 (103 aa)	<b>1 sheet</b> 2 beta hairpins, 3 strands <b>1 helix</b> 6 beta turns	7.69% 7.69%
	MRPL50	1–158 (158 aa)	<b>1 sheet</b> 1 strand <b>5 helices</b> 4 helix–helix interactions, 10 beta turns	5.88% 29.41%
	MRPS30	1–439 (439 aa)	<b>2 sheets</b> 1 beta alpha beta unit, 3 beta hairpins, 3 beta bulges, 12 strands <b>12 helices</b> 14 helix–helix interactions, 29 beta turns, 10 gamma turns	2.81% 16.90%
	Mitochondrial ATP synthase subunits	ATP6V1F	1–119 (119 aa)	<b>1 sheet</b> 2 beta alpha beta units, 1 beta bulge, 3 strands <b>4 helices</b> 6 helix–helix interactions, 17 beta turns, 3 gamma turns
NADH-ubiquinone oxidoreductases	MT-ND3	1–115 (115 aa)	<b>4 helices</b> 22 helix–helix interactions, 7 beta turns, 2 gamma turns	30.70%
	MT-ND6	1–174 (174 aa)	<b>9 helices</b> 30 helix–helix interactions, 12 beta turns, 6 gamma turns	33.33%
Cytochrome b-c1 complex subunits	UQCRH	17–91 (91 aa)	<b>4 helices</b> 7 helix–helix interactions, 5 beta turns, 1 gamma turn	40%
	UQCRI	2–63 (63 aa)	<b>3 helices</b> 6 helix–helix interactions, 6 beta turns	33.33%
HIG1 domain family member 1A, mitochondrial	HIGD1A	1–93 (93 aa)	<b>3 helices</b> 1 helix–helix interaction, 5 beta turns 7 gamma turns	20%
Dual specificity protein phosphatase 18	DUSP18	1–188 (188 aa)	<b>2 sheets</b> 2 beta hairpins, 1 beta bulge, 7 strands	6.25%
			<b>8 helices</b> 8 helix–helix interactions, 8 beta turns, 4 gamma turns	5.00%
Cytochrome c oxidase subunit 7B, mitochondrial	COX7B	30–78 (80 aa)	<b>1 helix</b> 3 helix–helix interactions, 2 beta turns	33.33%

The most significant KEGG (Kyoto Encyclopedia of Genes and Genomes) pathway enriched in our protein list was the oxidative phosphorylation pathway ( $p = 5.1 \times 10^{-5}$ , after Benjamini correction), which included 18 proteins from the list. In addition, there were three terms from the Biological Process sub-ontology of Gene Ontology (GO) [28,29] that were significantly enriched in our protein list (with  $p \leq 0.05$  after Benjamini correction): (i) chromatin silencing ( $p = 8.4 \times 10^{-6}$ ), with 13 proteins; (ii) mitochondrial electron transport, specifically NADH to ubiquinone ( $p = 1.2 \times 10^{-3}$ ), with 11 proteins; and (iii) mitochondrial respiratory chain complex I assembly ( $p = 8.9 \times 10^{-3}$ ), with 11 proteins from our list.

### PPI Networks

In the next part of this work, we focus on the products of genes previously shown to be involved in ovarian cancerogenesis and annotated in the Human Phenotype Ontology (HPO) list with the term Ovarian neoplasm (HP:0100615) [30]. Sixty-one genes on the HPO list were available online [31]. Since proteins do not act alone in the cell but rather make connections with other proteins to perform their functions, we aimed to predict whether RuCN targets some of the proteins in the PPI networks of these 61 ovarian-related

proteins from the HPO list. For this purpose, we used the String database of PPIs [32], with settings adjusted to retrieve only PPIs obtained from experiments (the active interaction source) and 100 interactors to be shown as the maximum number. The PPI network was searched for proteins whose interactors were predicted to be RuCN targets via the ISM. Three ovarian-related proteins had five or more proteins in their PPI networks identified as targets by ISM, AKT1, MDM2, and PRKN (Table 2). This result implies that the functions and pathways in which these proteins are involved are the most affected by RuCN.

**Table 2.** ISM-identified potential protein targets in String PPI networks of proteins annotated with the term “Ovarian neoplasm” (HP:0100615) in HPO (HPO proteins).

HPO Protein	ISM Protein in the PPI Network of HPO Protein	S/N Value in the CS of ISM Protein and RuCN
MDM2 (6)	YWHAQ	11.68431
	RASSF3	9.9321
	SFN(AKT1)—2	8.26526
	UBE2E3	7.55273
	ARRB1 (PRKN)—2	7.40497
	YWHAZ (AKT1, FGFR2)—3	6.60843
PRKN (6)	SQSTM1	13.47355
	LIMK1	11.41166
	PSMB4	10.03283
	RHOT2	9.66055
	CDK5	7.97013
	ARRB1 (MDM2)—2	7.40497
AKT1 (5)	SFN (MDM2)—2	8.26526
	HSPB1 (TP53)—2	8.24698
	SMAD3 (SMAD4, TGFBR2)—3	8.13051
	EGLN1	7.58537
	YWHAZ (FGFR2, MDM2)—3	6.60843
SMAD4 (4)	KDM6B	14.78335
	ACVR1B (TGFBR2)—2	9.87143
	RAN	9.42564
	SMAD3 (AKT1, TGFBR2)—3	8.13051
BRCA1 (3)	ACACA	10.60752
	TERF2IP (MRE11, NBN, RAD50)—4	9.37372
	FAM111A	6.8921
CTNNB1 (3)	BCL9	13.42896
	CTNNA1 (CDH1)—2	10.23149
	PSEN2	8.155
TP53 (3)	BAK1	16.43688
	HSPB1 (AKT1)—2	8.24698
	BCL2L2	7.12573
MRE11 (2)	TERF2IP (BRCA1, NBN, RAD50)—4	9.37372
	CHAMP1 (RAD50)—2	9.33687
RAD50 (2)	TERF2IP (BRCA1, MRE11, NBN)—4	9.37372
	CHAMP1 (MRE11)—2	9.33687
TGFBR2 (2)	ACVR1B (SMAD4)—2	9.87143
	SMAD3 (AKT1, SMAD4)—3	8.13051
CDH1 (1)	CTNNA1 (CTNNB1)—2	10.23149
CDKN2A (1)	PSMC3	7.13755
CHEK2 (1)	GINS2	6.01104
DICER1 (1)	TARBP2	6.7722
EWSR1 (1)	EIF4H	10.70126
FGFR2 (1)	YWHAZ (AKT1, MDM2)—3	6.60843
GATA4 (1)	FOS	11.15809
IDH1 (1)	DAZAP1	10.26606
LMNA (1)	LMNB2	11.67122
MSH2 (1)	FBXO5	8.00492
NBN (1)	TERF2IP (BRCA1, MRE11, RAD50)—4	9.37372
PALB2 (1)	MORF4L2	8.04956
RAD51 (1)	RAD51AP1	14.51291
RAD51D (1)	AMOTL2	7.63458

Most of the ISM targets present in the PPI networks of the ovarian-neoplasm-related proteins were specific for one network, suggesting that the interaction of RuCN with these proteins has a specific effect on the cells. Nevertheless, the proteins SMAD3, TERF2IP, and YWHAZ were present in three and four PPI networks (Table 2), indicating that RuCN's interaction with these proteins could affect several pathways within the cell. The ISM target SMAD3 is part of the PPI networks of AKT1, SMAD4, and TGFBR2. TERF2IP is a member of the PPI networks of BRCA1, MRE11, NBN, and RAD50. YWHAZ is an interactor with AKT1, FGFR2, and MDM2.

The most-affected PPI networks (AKT1, MDM2, and PRKN) by RuCN and RuCN/(N)-CDs drive central signalling cascades critical in tumorigenesis. These PPI networks, involving different types of proteins, are often deregulated in multiple malignancies and considered essential targets for developing selective inhibitors to suppress cancer growth and/or disease progression. The MDM2/p53 PPI inhibitors, RG7112 and RO5503781, were the first to enter clinical trials for patients with advanced malignancies [33]. The success of potent MDM2/p53 PPI inhibitors has significantly sped up studies seeking to target other PPIs with chemical agents acting as anticancer drugs. AKT1 is mainly involved in several critical cellular pathways, including regulating cell growth and division; therefore, it has been validated as a promising therapeutic target [34]. Similar to the other two networks, PRKN controls cell growth, metabolism, differentiation, and apoptosis [11].

### 3.2. $\mu$ FTIR Spectroscopy Study of Alterations of Cancer Cell Proteins' Secondary Structures

After identifying potential RuCN protein targets and PPI networks (as discussed in the previous section), we focused on the proteins' conformational changes in the cells and changes induced by RuCN without and with NCs (RuCN/CDs and RuCN/N-CDs). Interactions between drugs and proteins could alter secondary structures, folding, and protein functions. Consequently, protein structure changes provide insight into cancer cells' responses to a drug. We aimed to investigate if adding NCs (CDs or N-CDs) tunes the mechanism of RuCN and whether the drug's mode of action could be identified. To study changes in protein secondary structures, we applied FTIR, which generates a spectral signature of the macromolecular vibrations of a cell's entire contents. This cell-specific signature is sensitive even to slight variations in chemical content and the 2D structures of proteins [35,36]. An infrared (IR) protein signature of the potential drug and its nanotherapeutic effects was defined as all the spectral variations in the protein fingerprint region of a cell due to a RuCN, RuCN/CDs, and RuCN/N-CDs exposure, respectively. Therefore, we recorded the IR spectra of untreated cancer cells and compared them to the spectra of the treated A2780 cells (Figure 2a).

Proteins exhibit nine characteristic groups of frequencies in their IR spectra. These groups arise from the polypeptide repeat units, distributed as follows: Amide A ( $\sim 3300\text{ cm}^{-1}$ ), Amide B ( $3030\text{--}3100\text{ cm}^{-1}$ ), Amide I ( $\sim 1650\text{ cm}^{-1}$ ), Amide II ( $\sim 1550\text{ cm}^{-1}$ ), Amide III ( $1200\text{--}1400\text{ cm}^{-1}$ ), Amide IV ( $\sim 735\text{ cm}^{-1}$ ), Amide V ( $\sim 635\text{ cm}^{-1}$ ), Amide VI ( $\sim 600\text{ cm}^{-1}$ ), and Amide VII ( $\sim 200\text{ cm}^{-1}$ ) (Figure S1 and Table S2) [37,38]. Except for Amide I and II, amide bands are of little use in protein structural analysis due to their complexity and dependence on the nature of side chains and hydrogen bonding. Therefore, analyses of the spectral difference between untreated and treated cells are mainly based on the Amide I and II spectral band regions ( $1480\text{--}1700\text{ cm}^{-1}$ ) arising from C=O and C-N stretching vibrations, respectively, which will be addressed in this work.

Significant changes in spectra were observed after RuCN and RuCN/N-CDs treatment (Figure 2a), a result that was also confirmed by statistical analysis (Figure 2b), whereas RuCN/CDs did not affect cell protein structure. The most pronounced spectral differences compared to the control cells were observed as shifts in the position and intensity of the Amide I band and changes in the shape and intensity of the Amide II band after RuCN/N-CD treatment (Figure 2a). The Amide I and II band area was significantly reduced after the treatment with RuCN, while the RuCN/N-CDs positively affected the total protein content compared to control cells (Figure 2b), implying probable *de novo* synthesis of the proteins.



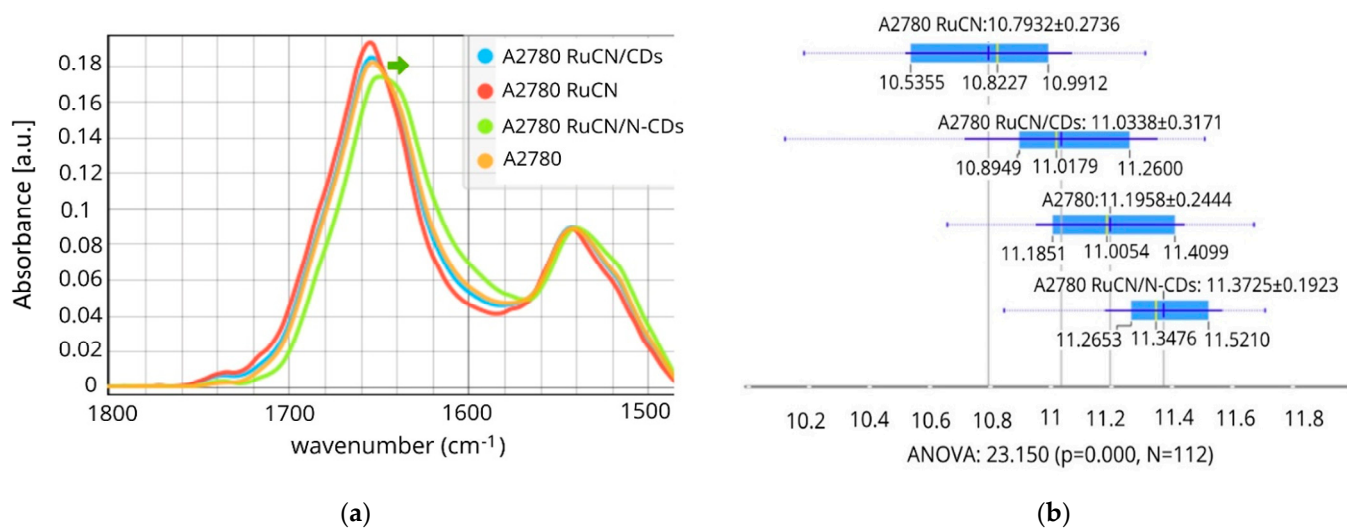


**Figure 2.** The  $\mu$ FTIR spectra of Amide I and Amide II regions, including the ester groups ( $1480\text{--}1800\text{ cm}^{-1}$ ). (a) Differences in the area of Amide I integration peaks ( $1600$  and  $1700\text{ cm}^{-1}$ ) (b). A green arrow indicates the downshift of the Amide I band after RuCN/N-CD treatment. (A2780 (control),  $N = 28$ ; A2780 RuCN-treated cells,  $N = 28$ ; A2780 treated with RuCN/CDs,  $N = 28$ ; and A2780 treated with RuCN/N-CDs,  $N = 28$ ).  $p < 0.05$  represents a statistically significant difference.

However, one can assume that an increase in the Amide I + Amide II area is caused by the superposition of protein- and N-CD-related signals. Namely, the FTIR spectra of CDs reveal a band at  $1639\text{ cm}^{-1}$  caused by the presence of carbonyls ( $\text{C}=\text{O}$ ) on the surface [19], while N-CDs have a band of a very strong intensity at  $1647\text{ cm}^{-1}$  assigned to a  $\text{C}=\text{O}$  stretching vibration in primary and/or tertiary amides [39]. Both signals are in the region of the Amide I band of proteins. Our study observed a decreased intensity of the Amide I band of proteins ( $\sim 1650\text{ cm}^{-1}$ ), as shown in Figure S1B, after treatment with N-CDs, whereas the treatment with CDs did not induce any changes in band intensity. If the observed changes were due to the superposition of signals from N-CDs or CDs, we would expect an increase in the intensity of the Amide I band because of the additive nature of overlapping peaks. Therefore, we can state that the decreased intensity of the Amide I band upon treatment with N-CDs indicates a deeper interaction mechanism between these NPs and proteins resulting in protein conformational changes.

Spectral shifting to lower wavenumbers was also observed, as the Amide I band of control cells ( $1651\text{ cm}^{-1}$ ) was shifted to  $1648\text{ cm}^{-1}$  after the RuCN/N-CDs treatment. This band is associated with the random coil structure, which emphasises protein structure changes after the treatment [38]. This pronounced content of random coil structures present after the RuCN/N-CDs treatment was also confirmed via Principal Component Analysis (PCA) (Figure S2). Furthermore, it was demonstrated earlier that hydrogen bonding with the amide  $\text{C}=\text{O}$  groups results in a shift of the Amide I bands to lower wavenumbers [40], which indicates that RuCN/N-CDs interact with proteins via hydrogen bonding. Such a spectral downshift of Amide I was not detected after the treatment with structural analogue without an N-CD carrier (RuCN treatment), which indicates that amino groups present on the surfaces of N-CDs are involved in hydrogen bonding with the  $\text{C}=\text{O}$  groups from proteins. Even though RuCN did not induce such prominent spectral variations, the treatment of cells with this transition metal complex caused secondary structural changes in cell proteins, which were noticeable as a decrease in the Amide I band area (Figure 2b).

#### Changes in Individual Secondary Structures of Proteins

The Amide I and II bands represent a mixture of secondary structure components characteristic of each cell type. Individual hidden absorption bands could be derived from the second-derivative spectra of Amides I and II. This approach allowed us to discern

subtle changes in the secondary structures, thereby providing a more comprehensive understanding of the treatment effects. The second-derivative of the Amide I and II bands ( $1480\text{--}1700\text{ cm}^{-1}$ ), as shown in Figure 3, revealed that these bands consist of six sub-bands: the parallel  $\beta$ -sheet ( $1635\text{ cm}^{-1}$ ), the  $\alpha$ -helix structure ( $1656\text{ cm}^{-1}$ ), turns and loops as well as antiparallel  $\beta$ -sheet structures ( $1685\text{ cm}^{-1}$ ), the  $\alpha$ -helix ( $1543\text{ cm}^{-1}$ ), tyrosine (Tyr) ( $1515\text{ cm}^{-1}$ ), and phenylalanine (Phe) ( $1495\text{ cm}^{-1}$ ) side chains of amino acids. The identified bands were assigned to the Amide I and II region using previously described spectral components associated with different secondary structures [41–45] and given in Table 3.

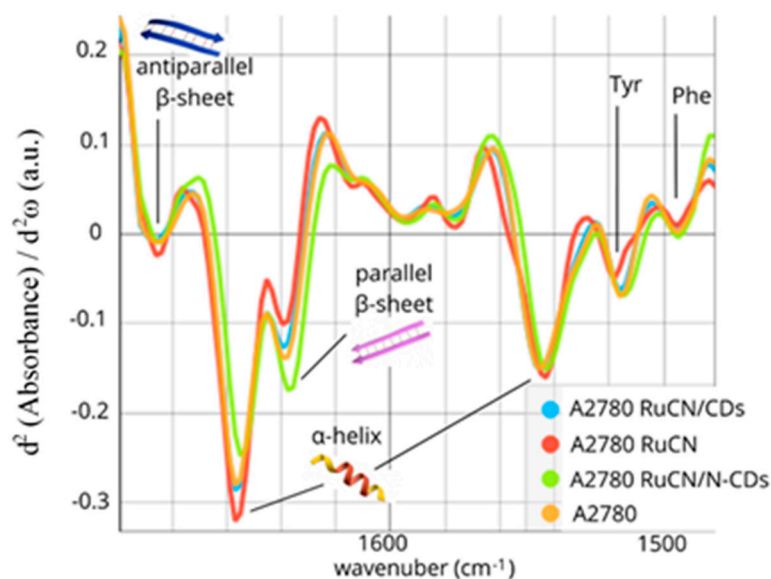


**Figure 3.** The second derivative of Amides I and II of the untreated cells (orange line) and cells treated with RuCN (red line), RuCN/CDs (blue line), and RuCN/N-CDs (green line).

**Table 3.** Correlation between Amide I and II peak frequency positions obtained from the secondary-derivative spectrum and secondary structure assignments.

Frequency ( $\text{cm}^{-1}$ )	Band Assignment
1685	Antiparallel $\beta$ -sheet
1656	$\alpha$ -helix
1635	Parallel $\beta$ -sheet
1543	$\alpha$ -helix
1515	Tyrosine (Tyr)
1495	Phenylalanine (Phe)

The following changes were detected after the RuCN treatment: an increase in  $\alpha$ -helix content and a decrease in parallel  $\beta$ -sheet content (Figure 3). On the contrary, a prominent increase in the number of parallel  $\beta$ -sheets and a reduction in the number of  $\alpha$ -helices were observed when RuCN with an N-CD carrier was applied (the RuCN/N-CD treatment). Besides the quantitative decrease in the number of  $\alpha$ -structures, their qualitative rearrangement was observed as a shift to the lower frequency (Figure 3). The interaction of cells with RuCN/N-CDs probably leads to a slight distortion in the  $\alpha$ -helix structure or/and, partly, a  $\alpha$ -helix–random coil transition. Changes in tertiary structure, resulting from changes in the relative orientations of some helical segments, can also be excluded. However, 3D structural changes in proteins after their interaction with carbon quantum dots have already been hypothesised [46], most likely resulting in changes in protein function.

The treatment with RuCN/N-CDs also led to the following modifications in the Amide II region related to aromatic amino acid residues: (i) a significantly increased contribution of the band area at  $\approx 1515\text{ cm}^{-1}$ , i.e., of the “shoulder” peak associated with tyrosine (Tyr) indole ring vibrations (Figure 2a) [47], and (ii) a moderate increase in the band associated with phenylalanine (Phe) residue (Figure 3). In addition, the minimum position of PC2 at  $1588\text{ cm}^{-1}$ , which is related to the C—C stretching of phenyl rings, and the maximum at  $1503\text{ cm}^{-1}$ , which is associated with the C—H bending of phenyl rings [48,49], point to notable differences arising from the Phe residue as well (Figure S2). Moreover, an increase in the band at  $1161\text{ cm}^{-1}$  that arise from the stretching vibrations of hydrogen-bonded C-OH groups of serine (Ser), threonine (Thr), and Tyr residues of cellular proteins was detected [50–53] (Figure S1B). Previously, the peaks at  $1161$  and  $1172\text{ cm}^{-1}$  that originate mainly from the C-OH groups of Ser, Thr, and Tyr residues were observed in MCF-7 cells (from the human breast adenocarcinoma cell line) and colon tissues as well [53,54]. The importance of the -OH groups of these three amino acids is that they can be phosphorylated by several oncoproteins and, therefore, involved in essential signalling mechanisms that drive malignant cell characteristics [55]. As the cited authors indicated, the component bands at  $1161\text{ cm}^{-1}$  arise from the stretching vibrations of hydrogen-bonded C-O groups, whereas the band at  $1172\text{ cm}^{-1}$  is due to the stretching vibrations of non-hydrogen-bonded C-O groups. This result implies higher quantities of hydrogen-bonded Ser, Thr, and Tyr residues after RuCN/N-CDs treatment. These new hydrogen bonds could be formed between amino groups on N-CDs’ surface and -OH groups originating from Ser, Thr, and Tyr protein residues. The hydrogen bonding between amino groups from N-CD carriers and protein C=O groups was also ascribed to be the leading cause of the Amide I spectral downshift (Figure 2a).

### 3.3. Synergy of Bioinformatics and the FTIR Micro-Spectroscopy Approach

We used computational biology to identify specific protein targets for the anticancer drug RuCN and CD carriers for drug delivery and FTIR spectroscopy to provide a comprehensive understanding of their impact on cancer cell protein structure. In the next phase, we leveraged computational biology tools to elucidate structural changes’ underlying mechanisms and potential biological implications.

The most statistically significant change in the FTIR spectra after the RuCN/N-CD treatment was the parallel  $\beta$ -sheet increase (Figures Figure 3 and S2). This increase could be caused either by the stabilisation of  $\beta$ -sheet structures via protein interactions with RuCN/N-CDs (or treatment-induced “stabilisation factors”) or by the alterations in the expression levels and the de novo synthesis of proteins rich in the  $\beta$ -sheet structure after the treatment [56]. To reveal potential protein targets more precisely, we narrowed the number of possible mitochondrion-related proteins with the highest DAVID enrichment score to those with the highest content of the  $\beta$ -sheet structures (Table 1), and NDUFS1 stood out as the protein that could be overproduced after treatment or the most affected target protein for interaction with RuCN/N-CDs.

In the same way, the  $\alpha$ -helix-rich proteins NDUF1 and NDUF5 stood out as potentially overexpressed proteins after RuCN treatment. An alternate option is stabilising helical structures in protein targets for RuCN through the interaction with the transition metal complex.

Furthermore, treating cells with RuCN/CDs did not induce any significant changes in the protein secondary structure, implying that Ru metallodrug interaction with CDs might sustain the coordination of RuCN with proteins.

We have shown that adding N-CDs to RuCN induces structural changes in proteins differently than the potential drug alone, implying there are different target molecules and therapeutic modalities. Even though the tested compounds had different protein targets (the suggested target proteins for RuCN are NDUF1 and NDUF5, and the target for RuCN/N-CDs is NDUFS1), the target proteins belong to the same protein groups, called NADH dehydrogenases. These enzymes play a crucial role in cellular respiration

and energy production. Actively proliferating cancer cells require substantial amounts of NADH and NADPH. Therefore, selectively lowering NADH and NADPH levels is a promising cancer treatment strategy. Targeting these enzymes and their associated pathways has already been extensively studied as a potential therapeutic strategy for cancer treatment [57].

The effect observed in this work could be related to the results presented in our previous work [58], in which we demonstrated that coordination of the potential drug RuCN to an N-CD NC suppresses the level of oxidative stress while still maintaining the drug's antitumor activity and potential to penetrate through the cell membrane. Therefore, it could be that combining this Ru drug with N-CD carriers balances the anticancer efficiency and leads to better therapeutical outcomes by reducing the oxidative stress linked to cancer progression, thus reducing the level of necrosis and inflammatory response. Additional therapeutical mechanisms might be the specific alterations in the protein secondary structure that the N-CDs in the nanocomposite system enable through specific interactions with the target NDUFS1 protein rich in  $\beta$ -sheet structures.

This combined approach enables the precise identification of protein targets for anticancer drugs through advanced computational models, facilitating tailored drug design.

#### 4. Conclusions

Mitochondrion-related proteins were identified as potential targets for RuCN and RuCN/N-CDs. Interaction with the mentioned proteins might destabilise AKT1, MDM2, and PRKN signalling pathways, which control cancer cells' survival, proliferation, invasion, apoptosis, and angiogenesis, making the combined drug's therapeutic effect promising. We have demonstrated that combining RuCN with NCs may play a role in fine-tuning drug action and directing this drug toward a specific protein target through distinct interactions.

The results presented in this manuscript reveal that the treatment of ovarian cancer cells with RuCN induced a higher content of  $\alpha$ -helices and a lower content of  $\beta$ -sheet structures compared to the untreated control and the overexpression of NDUFA1 and NDUFB5, respectively. On the other hand, coordination of the RuCN to the CD NCs blocked the coordination ability of the RuCN and did not affect the protein secondary structure of the A2780 cancer cell line. Furthermore, using N-CDs as NCs for the RuCN induced quite the opposite alterations in the secondary structures of ovarian cancer cellular proteins compared to those induced by the drug RuCN itself, which implies there are other protein targets for coordination and different therapeutic modalities. A substantially higher content of parallel  $\beta$ -sheets was observed, which highlighted  $\beta$ -sheet-rich protein NDUFS1 as the protein that could be overproduced after treatment or the most affected target protein for interaction with RuCN/N-CDs through the specific hydrogen bonding of the amino group from N-CDs with the protein C=O groups and -OH groups of Ser, Thr, and Tyr residues. Therefore, the correct choice of NC can provide new tools for further improvement, adaptation, and fine adjustment of drugs for specific protein targets in anticancer treatments. This could lead to rationally designed anticancer drug nanosystems targeting specific biomolecules or/and molecular events.

**Supplementary Materials:** The following supporting information can be downloaded at: <https://www.mdpi.com/article/10.3390/pharmaceutics16080997/s1>, Figure S1: SR-FTIR spectra of Amide A, Amide B, (A) Amide I, II, and III regions (B) characteristic for protein analysis; Figure S2: PCA scores plot (A) and corresponding PCA loadings profile (B) of the second derivative data of the spectral region ( $1500\text{--}1700\text{ cm}^{-1}$ ) of control (orange) untreated cells, and cells treated with RuCN (red), RuCN/N-CDs (green) and RuCN/CDs (blue); Table S1: DAVID enrichment analysis on proteins identified as potential targets of RuCN; clusters with the highest Enrichment scores are shown; Table S2: Assignments of peak positions.

**Author Contributions:** M.D.N. and M.P.: Conceptualisation. M.D.N., T.D., B.G. and M.P., Methodology. M.D.N., T.D., M.S. (Milan Senčanski) and B.G.: Formal Analysis. T.D., M.D.N., M.A., B.G., M.G. and M.P.: Investigation. T.D. and M.D.N.: Data Curation. M.D.N.: Writing—Original Draft

Preparation. M.S. (Milutin Stepić), M.S. (Milan Senćanski), T.D., B.G., M.A., I.A.P., Đ.K. and M.P.: Writing—Review and Editing. M.D.N., I.A.P. and M.S. (Milutin Stepić): Visualization. M.P. and T.D.: Supervision. All authors have read and agreed to the published version of the manuscript.

**Funding:** The research was funded by the Ministry of Science, Technological Development and Innovation of the Republic of Serbia (451-03-66/2024-03/200017). The authors are grateful for financial support from the Spanish Ministry of Science and Innovation (MCIN/AEI/10.13039/501100011033) through project PID2021-122613OB-I00, and also to FCT (CQM Base Fund—UIDB/00674/2020, Programmatic Fund—UIDP/00674/2020); Madeira 14-20 Program (project Reforço do Investimento Equipamentos e Infrastructures Científicasna RAM (PROEQUIPRAM) M1420-01-0145-FEDER-000008); and Agência Regional para o Desenvolvimento da Investigação, Tecnologia e Inovação (ARDITI) through the ARDITI-CQM/2018/007-PDG (Fellowship Grant to M.G.), project M1420-01-0145-FEDER-000005-CQM+ (Madeira 14–20).

**Institutional Review Board Statement:** Not applicable.

**Informed Consent Statement:** Not applicable.

**Data Availability Statement:** Data will be made available at a reasonable request.

**Acknowledgments:** These experiments were performed at MIRAS beamline at ALBA Synchrotron with the collaboration of ALBA staff (experiment No. 2019093770).

**Conflicts of Interest:** The authors declare no conflicts of interest.

## References

1. Desai, A.; Xu, J.; Aysola, K.; Qin, Y.; Okoli, C.; Hariprasad, R.; Chinemerem, U.; Gates, C.; Reddy, A.; Danner, O.; et al. Epithelial Ovarian Cancer: An Overview. *World J. Transl. Med.* **2014**, *3*, 1–8. [[CrossRef](#)] [[PubMed](#)]
2. Gavas, S.; Quazi, S.; Karpiński, T.M. Nanoparticles for Cancer Therapy: Current Progress and Challenges. *Nanoscale Res. Lett.* **2021**, *16*, 173. [[CrossRef](#)] [[PubMed](#)]
3. Bhatia, S.N.; Chen, X.; Dobrovolskaia, M.A.; Lammers, T. Cancer Nanomedicine. *Nat. Rev. Cancer* **2022**, *22*, 550–556. [[CrossRef](#)]
4. Attia, M.F.; Anton, N.; Wallyn, J.; Omran, Z.; Vandamme, T.F. An Overview of Active and Passive Targeting Strategies to Improve the Nanocarriers Efficiency to Tumour Sites. *J. Pharm. Pharmacol.* **2019**, *71*, 1185–1198. [[CrossRef](#)]
5. Bazak, R.; Hourri, M.; Achy, S.E.; Hussein, W.; Refaat, T. Passive Targeting of Nanoparticles to Cancer: A Comprehensive Review of the Literature. *Mol. Clin. Oncol.* **2014**, *2*, 904–908. [[CrossRef](#)] [[PubMed](#)]
6. Zhou, Y.; Lih, T.M.; Pan, J.; Höti, N.; Dong, M.; Cao, L.; Hu, Y.; Cho, K.-C.; Chen, S.-Y.; Eguez, R.V.; et al. Proteomic Signatures of 16 Major Types of Human Cancer Reveal Universal and Cancer-Type-Specific Proteins for the Identification of Potential Therapeutic Targets. *J. Hematol. Oncol.* **2020**, *13*, 170. [[CrossRef](#)] [[PubMed](#)]
7. van der Watt, P.J.; Ngarande, E.; Leaner, V.D. Overexpression of Kpn $\beta$ 1 and Kpn $\alpha$ 2 Importin Proteins in Cancer Derives from Deregulated E2F Activity. *PLoS ONE* **2011**, *6*, e27723. [[CrossRef](#)] [[PubMed](#)]
8. Li, S.; Huang, S.; Peng, S.-B. Overexpression of G Protein-Coupled Receptors in Cancer Cells: Involvement in Tumor Progression. *Int. J. Oncol.* **2005**, *27*, 1329–1338. [[CrossRef](#)]
9. Schmit, K.; Michiels, C. TMEM Proteins in Cancer: A Review. *Front. Pharmacol.* **2018**, *9*, 1345. [[CrossRef](#)]
10. Otto, T.; Sicinski, P. Cell Cycle Proteins as Promising Targets in Cancer Therapy. *Nat. Rev. Cancer* **2017**, *17*, 93–115. [[CrossRef](#)]
11. Fabbro, D.; Ruetz, S.; Buchdunger, E.; Cowan-Jacob, S.W.; Fendrich, G.; Liebetanz, J.; Mestan, J.; O'Reilly, T.; Traxler, P.; Chaudhuri, B.; et al. Protein Kinases as Targets for Anticancer Agents: From Inhibitors to Useful Drugs. *Pharmacol. Ther.* **2002**, *93*, 79–98. [[CrossRef](#)] [[PubMed](#)]
12. Golbaghi, G.; Pitard, I.; Lucas, M.; Haghdoost, M.M.; de Los Santos, Y.L.; Doucet, N.; Patten, S.A.; Sanderson, J.T.; Castonguay, A. Synthesis and Biological Assessment of a Ruthenium(II) Cyclopentadienyl Complex in Breast Cancer Cells and on the Development of Zebrafish Embryos. *Eur. J. Med. Chem.* **2020**, *188*, 112030. [[CrossRef](#)] [[PubMed](#)]
13. Bruce, M.I.; Windsor, N.J. Cyclopentadienyl-Ruthenium and -Osmium Chemistry. IV. Convenient High-Yield Synthesis of Some Cyclopentadienyl Ruthenium or Osmium Tertiary Phosphine Halide Complexes. *Aust. J. Chem.* **1977**, *30*, 1601–1604. [[CrossRef](#)]
14. Gill, T.P.; Mann, K.R. Photochemical Properties of the Cyclopentadienyl(eta-6-Benzene)Ruthenium(II) Cation. The Synthesis and Reactions of a Synthetically Useful Intermediate: The Cyclopentadienyltris(Acetonitrile)Ruthenium(II) Cation. *Organometallics* **1982**, *1*, 485–488. [[CrossRef](#)]
15. Streu, C.; Carroll, P.J.; Kohli, R.K.; Meggers, E. Synthesis of Cyclopentadienyl Ruthenium Complexes Bearing Pendant Chelating Picolinates through an Electrophilic Precursor. *J. Organomet. Chem.* **2008**, *693*, 551–556. [[CrossRef](#)] [[PubMed](#)]
16. Bregman, H.; Meggers, E. Ruthenium Half-Sandwich Complexes as Protein Kinase Inhibitors: An N-Succinimidyl Ester for Rapid Derivatizations of the Cyclopentadienyl Moiety. *Org. Lett.* **2006**, *8*, 5465–5468. [[CrossRef](#)] [[PubMed](#)]
17. Zhang, L.; Carroll, P.; Meggers, E. Ruthenium Complexes as Protein Kinase Inhibitors. *Org. Lett.* **2004**, *6*, 521–523. [[CrossRef](#)] [[PubMed](#)]

18. Nešić, M.D.; Dučić, T.; Gonçalves, M.; Stepić, M.; Algarra, M.; Soto, J.; Gemović, B.; Bandosz, T.J.; Petković, M. Biochemical Changes in Cancer Cells Induced by Photoactive Nanosystem Based on Carbon Dots Loaded with Ru-Complex. *Chem.-Biol. Interact.* **2022**, *360*, 109950. [CrossRef]
19. Algarra, M.; Campos, B.; Radotic, K.; Mutavdzic, D.; Bandosz, T.; Jimenez-Jimenez, J.; Rodriguez-Castellon, E.; Esteves da Silva, J. Luminescent Carbon Nanoparticles: Effects of Chemical Functionalization, and Evaluation of Ag<sup>+</sup> Sensing Properties. *J. Mater. Chem. A* **2014**, *2*, 8342–8351. [CrossRef]
20. Houdová, D.; Soto, J.; Castro, R.; Rodrigues, J.; Soledad Pino-González, M.; Petković, M.; Bandosz, T.J.; Algarra, M. Chemically Heterogeneous Carbon Dots Enhanced Cholesterol Detection by MALDI TOF Mass Spectrometry. *J. Colloid Interface Sci.* **2021**, *591*, 373–383. [CrossRef]
21. Veljkovic, V.A. *Theoretical Approach to the Preselection of Carcinogens and Chemical Carcinogenesis*; Gordon and Breach Science Publishers: London, UK, 1980; ISBN 978-0-677-05490-2.
22. Sencanski, M.; Perovic, V.; Pajovic, S.B.; Adzic, M.; Paessler, S.; Glisic, S. Drug Repurposing for Candidate SARS-CoV-2 Main Protease Inhibitors by a Novel In Silico Method. *Molecules* **2020**, *25*, 3830. [CrossRef]
23. Papatheodorou, I.; Moreno, P.; Manning, J.; Fuentes, A.M.-P.; George, N.; Fexova, S.; Fonseca, N.A.; Füllgrabe, A.; Green, M.; Huang, N.; et al. Expression Atlas Update: From Tissues to Single Cells. *Nucleic Acids Res.* **2020**, *48*, D77–D83. [CrossRef] [PubMed]
24. Veljković, N.V.; Glišić, S.; Prlić, J.; Perović, V.R.; Botta, M.; Veljković, V. Discovery of New Therapeutic Targets by the Informational Spectrum Method. *Curr. Protein Pept. Sci.* **2008**, *9*, 493–506. [CrossRef] [PubMed]
25. Veljkovic, N.; Glisic, S.; Perovic, V.; Veljkovic, V. The Role of Long-Range Intermolecular Interactions in Discovery of New Drugs. *Expert Opin. Drug Discov.* **2011**, *6*, 1263–1270. [CrossRef] [PubMed]
26. Ma, X.; Xiong, Y.; Lee, L.T.O. Application of Nanoparticles for Targeting G Protein-Coupled Receptors. *Int. J. Mol. Sci.* **2018**, *19*, 2006. [CrossRef] [PubMed]
27. Sherman, B.T.; Hao, M.; Qiu, J.; Jiao, X.; Baseler, M.W.; Lane, H.C.; Imamichi, T.; Chang, W. DAVID: A Web Server for Functional Enrichment Analysis and Functional Annotation of Gene Lists (2021 Update). *Nucleic Acids Res.* **2022**, *50*, W216–W221. [CrossRef] [PubMed]
28. Ashburner, M.; Ball, C.A.; Blake, J.A.; Botstein, D.; Butler, H.; Cherry, J.M.; Davis, A.P.; Dolinski, K.; Dwight, S.S.; Eppig, J.T.; et al. Gene Ontology: Tool for the Unification of Biology. The Gene Ontology Consortium. *Nat. Genet.* **2000**, *25*, 25–29. [CrossRef] [PubMed]
29. Gene Ontology Consortium. The Gene Ontology Resource: Enriching a GOld Mine. *Nucleic Acids Res.* **2021**, *49*, D325–D334. [CrossRef]
30. Köhler, S.; Gargano, M.; Matentzoglou, N.; Carmody, L.C.; Lewis-Smith, D.; Vasilevsky, N.A.; Danis, D.; Balagura, G.; Baynam, G.; Brower, A.M.; et al. The Human Phenotype Ontology in 2021. *Nucleic Acids Res.* **2021**, *49*, D1207–D1217. [CrossRef]
31. Human Phenotype Ontology. Available online: <https://hpo.jax.org/app/browse/term/HP:0100615> (accessed on 16 April 2024).
32. Szklarczyk, D.; Gable, A.L.; Lyon, D.; Junge, A.; Wyder, S.; Huerta-Cepas, J.; Simonovic, M.; Doncheva, N.T.; Morris, J.H.; Bork, P.; et al. STRING V11: Protein-Protein Association Networks with Increased Coverage, Supporting Functional Discovery in Genome-Wide Experimental Datasets. *Nucleic Acids Res.* **2019**, *47*, D607–D613. [CrossRef]
33. Zhao, Y.; Aguilar, A.; Bernard, D.; Wang, S. Small-Molecule Inhibitors of the MDM2-P53 Protein-Protein Interaction (MDM2 Inhibitors) in Clinical Trials for Cancer Treatment. *J. Med. Chem.* **2015**, *58*, 1038–1052. [CrossRef]
34. Shariati, M.; Meric-Bernstam, F. Targeting AKT for Cancer Therapy. *Expert Opin. Investig. Drugs* **2019**, *28*, 977–988. [CrossRef] [PubMed]
35. Derenne, A.; Mignolet, A.; Goormaghtigh, E. FTIR Spectral Signature of Anticancer Drug Effects on PC-3 Cancer Cells: Is There Any Influence of the Cell Cycle? *Analyst* **2013**, *138*, 3998–4005. [CrossRef] [PubMed]
36. Mignolet, A.; Derenne, A.; Smolina, M.; Wood, B.R.; Goormaghtigh, E. FTIR Spectral Signature of Anticancer Drugs. Can Drug Mode of Action Be Identified? *Biochim. Biophys. Acta* **2016**, *1864*, 85–101. [CrossRef]
37. Krimm, S.; Bandekar, J. Vibrational Spectroscopy and Conformation of Peptides, Polypeptides, and Proteins. *Adv. Protein Chem.* **1986**, *38*, 181–364. [CrossRef]
38. Usoltsev, D.; Sitnikova, V.; Kajava, A.; Uspenskaya, M. Systematic FTIR Spectroscopy Study of the Secondary Structure Changes in Human Serum Albumin under Various Denaturation Conditions. *Biomolecules* **2019**, *9*, 359. [CrossRef] [PubMed]
39. Travlou, N.; Giannakoudakis, D.; Algarra, M.; Labella, A.; Rodriguez-Castellon, E.; Bandos, T. S- and N-doped carbon quantum dots: Surface chemistry dependent antibacterial activity. *Carbon* **2018**, *135*, 104–111. [CrossRef]
40. Myshakina, N.S.; Ahmed, Z.; Asher, S.A. Dependence of Amide Vibrations on Hydrogen Bonding. *J. Phys. Chem. B* **2008**, *112*, 11873–11877. [CrossRef]
41. Barth, A. Infrared Spectroscopy of Proteins. *Biochim. Biophys. Acta* **2007**, *1767*, 1073–1101. [CrossRef]
42. Fabian, H.; Naumann, D. (Eds.) *Protein Folding and Misfolding: Shining Light by Infrared Spectroscopy*; Biological and Medical Physics, Biomedical Engineering; Springer: Berlin/Heidelberg, Germany, 2012; ISBN 978-3-642-22229-0. [CrossRef]
43. Jackson, M.; Mantsch, H.H. The Use and Misuse of FTIR Spectroscopy in the Determination of Protein Structure. *Crit. Rev. Biochem. Mol. Biol.* **1995**, *30*, 95–120. [CrossRef]
44. Sadat, A.; Joye, I.J. Peak Fitting Applied to Fourier Transform Infrared and Raman Spectroscopic Analysis of Proteins. *Appl. Sci.* **2020**, *10*, 5918. [CrossRef]

45. Usoltsev, D.; Sitnikova, V.; Kajava, A.; Uspenskaya, M. FTIR Spectroscopy Study of the Secondary Structure Changes in Human Serum Albumin and Trypsin under Neutral Salts. *Biomolecules* **2020**, *10*, 606. [[CrossRef](#)]
46. Kunachowicz, D.; Ściskalska, M.; Jakubek, M.; Kizek, R.; Kepinska, M. Structural Changes in Selected Human Proteins Induced by Exposure to Quantum Dots, Their Biological Relevance and Possible Biomedical Applications. *NanoImpact* **2022**, *26*, 100405. [[CrossRef](#)]
47. Kreuzer, M.; Dučić, T.; Hawlina, M.; Andjelic, S. Synchrotron-Based FTIR Microspectroscopy of Protein Aggregation and Lipids Peroxidation Changes in Human Cataractous Lens Epithelial Cells. *Sci. Rep.* **2020**, *10*, 15489. [[CrossRef](#)] [[PubMed](#)]
48. Piccirilli, F.; Schirò, G.; Vetri, V.; Lupi, S.; Perucchi, A.; Militello, V. Decoding Vibrational States of Concanavalin A Amyloid Fibrils. *Biophys. Chem.* **2015**, *199*, 17–24. [[CrossRef](#)] [[PubMed](#)]
49. Titus, J.; Ghimire, H.; Viennois, E.; Merlin, D.; Unil Perera, A.G. Protein Secondary Structure Analysis of Dried Blood Serum Using Infrared Spectroscopy to Identify Markers for Colitis Screening. *J. Biophotonics* **2018**, *11*, e201700057. [[CrossRef](#)]
50. Bellisola, G.; Della Peruta, M.; Vezzalini, M.; Moratti, E.; Vaccari, L.; Birarda, G.; Piccinini, M.; Cinque, G.; Sorio, C. Tracking Infrared Signatures of Drugs in Cancer Cells by Fourier Transform Microspectroscopy. *Analyst* **2010**, *135*, 3077–3086. [[CrossRef](#)] [[PubMed](#)]
51. Movasaghi, Z.; Rehman, S.; Ur Rehman, D.I. Fourier Transform Infrared (FTIR) Spectroscopy of Biological Tissues. *Appl. Spectrosc. Rev.* **2008**, *43*, 134–179. [[CrossRef](#)]
52. Wong, P.T.; Wong, R.K.; Caputo, T.A.; Godwin, T.A.; Rigas, B. Infrared Spectroscopy of Exfoliated Human Cervical Cells: Evidence of Extensive Structural Changes during Carcinogenesis. *Proc. Natl. Acad. Sci. USA* **1991**, *88*, 10988–10992. [[CrossRef](#)]
53. Wu, B.-B.; Gong, Y.-P.; Wu, X.-H.; Chen, Y.-Y.; Chen, F.-F.; Jin, L.-T.; Cheng, B.-R.; Hu, F.; Xiong, B. Fourier Transform Infrared Spectroscopy for the Distinction of MCF-7 Cells Treated with Different Concentrations of 5-Fluorouracil. *J. Transl. Med.* **2015**, *13*, 108. [[CrossRef](#)]
54. Rigas, B.; Morgello, S.; Goldman, I.S.; Wong, P.T. Human Colorectal Cancers Display Abnormal Fourier-Transform Infrared Spectra. *Proc. Natl. Acad. Sci. USA* **1990**, *87*, 8140–8144. [[CrossRef](#)]
55. Bishop, J.M. Viral Oncogenes. *Cell* **1985**, *42*, 23–38. [[CrossRef](#)]
56. Veena, M.S.; Wilken, R.; Zheng, J.-Y.; Gholkar, A.; Venkatesan, N.; Vira, D.; Ahmed, S.; Basak, S.K.; Dalgard, C.L.; Ravichandran, S.; et al. P16 Protein and Gigaxonin Are Associated with the Ubiquitination of NFκB in Cisplatin-Induced Senescence of Cancer Cells. *J. Biol. Chem.* **2014**, *289*, 34921–34937. [[CrossRef](#)]
57. Pramono, A.A.; Rather, G.M.; Herman, H.; Lestari, K.; Bertino, J.R. NAD- and NADPH-Contributing Enzymes as Therapeutic Targets in Cancer: An Overview. *Biomolecules* **2020**, *10*, 358. [[CrossRef](#)]
58. Nešić, M.D.; Dučić, T.; Algarra, M.; Popović, I.; Stepić, M.; Gonçalves, M.; Petković, M. Lipid Status of A2780 Ovarian Cancer Cells after Treatment with Ruthenium Complex Modified with Carbon Dot Nanocarriers: A Multimodal SR-FTIR Spectroscopy and MALDI TOF Mass Spectrometry Study. *Cancers* **2022**, *14*, 1182. [[CrossRef](#)]

**Disclaimer/Publisher’s Note:** The statements, opinions and data contained in all publications are solely those of the individual author(s) and contributor(s) and not of MDPI and/or the editor(s). MDPI and/or the editor(s) disclaim responsibility for any injury to people or property resulting from any ideas, methods, instructions or products referred to in the content.